January 2003

A magneto-hydrodynamically controlled fluidic network

Haim H. Bau
University of Pennsylvania, bau@seas.upenn.edu

Jianzhong Zhu
University of Pennsylvania

Shizhi Qian
University of Pennsylvania

Yu Zhiang
University of Pennsylvania

Postprint version. Published in *Sensors and Actuators B: Chemical*, Volume 88, Issue 2, January 2003, pages 205-216.
Publisher URL: http://dx.doi.org/10.1016/S0925-4005(02)00325-8

A magneto-hydrodynamically controlled fluidic network

Abstract
The paper describes fluidic networks consisting of individually controlled branches. The networks' basic building blocks are conduits equipped with two electrodes positioned on opposing walls. The entire device is either subjected to an external uniform magnetic field or fabricated within a magnetic material. When a prescribed potential difference is applied across each electrode pair, it induces current in the liquid (assumed to be at least a weak electrolyte solution). Analogously with electric circuits, by judicious application of the potential differences at various branches, one can direct liquid flow in any desired way without a need for mechanical pumps or valves. Equipped with additional, internally located electrodes, the network branches double as stirrers capable of generating chaotic advection. The paper describes the basic building blocks for such a network, the operation of these branches as stirrers, a general linear graph-based theory for the analysis and optimal control of fluidic magneto-hydrodynamic networks, an example of a network fabricated with low temperature, co-fired ceramic tapes, and preliminary experimental observations that illustrate that the ideas described in this paper can, indeed, be implemented in practice.

Keywords
microfluidic networks, chaotic stirring, magneto hydro dynamics, MHD, micro pump, micro mixer

Comments
Postprint version. Published in *Sensors and Actuators B: Chemical*, Volume 88, Issue 2, January 2003, pages 205-216.
Publisher URL: http://dx.doi.org/10.1016/S0925-4005(02)00325-8

Bau, H., H., Zhu, J., Qian, S., and Xiang, Y., 2003, A Magneto-Hydrodynamically Controlled Fluidic Network, Sensors and Actuators B: Chemical, 88, 205-216.

A MAGNETO-HYDRODYNAMICALLY CONTROLLED FLUIDIC NETWORK

Haim H. Bau*, Jianzhong Zhu, Shizhi Qian, and Yu Xiang

Department of Mechanical Engineering and Applied Mechanics
University of Pennsylvania, Philadelphia, PA 19104-6315, USA
e-mail: bau@seas.upenn.edu Fax: 215-573-6334

ABSTRACT

The paper describes fluidic networks consisting of individually controlled branches. The networks' basic building blocks are conduits equipped with two electrodes positioned on opposing walls. The entire device is either subjected to an external uniform magnetic field or fabricated within a magnetic material. When a prescribed potential difference is applied across each electrode pair, it induces current in the liquid (assumed to be at least a weak electrolyte solution). Analogously with electric circuits, by judicious application of the potential differences at various branches, one can direct liquid flow in any desired way without a need for mechanical pumps or valves. Equipped with additional, internally located electrodes, the network branches double as stirrers capable of generating chaotic advection. The paper describes the basic building blocks for such a network, the operation of these branches as stirrers, a general linear graph-based theory for the analysis and optimal control of fluidic magneto-hydrodynamic networks, an example of a network fabricated with low temperature, co-fired ceramic tapes, and preliminary experimental observations that illustrate that the ideas described in this paper can, indeed, be implemented in practice.

Keywords: Microfluidic networks, Chaotic Stirring, Magneto Hydro Dynamics, MHD, Micro Pump, Micro Mixer

* All correspondence should be directed to this author.

1. **INTRODUCTION**

In recent years, there has been a growing interest in developing minute chemical and biological laboratories, analytical devices, and reactors. Often it is necessary to propel fluids from one part of the device to another, control the fluid motion, stir, and separate fluids. In microdevices, these tasks are far from trivial. Frequently, electrostatic forces are being used to move liquids around. These forces usually induce only very low flow rates, require the use of high electrical potentials, and may cause significant heating of the solution. The use of electromagnetic forces presents an interesting and flexible means for manipulating liquids in micro fluidic devices and systems. The only requirement is that the liquid be at least slightly conductive-a requirement that is met by many biological solutions.

The application of electromagnetic forces to pump, confine, and control fluids is not new. The field is generally known as Magneto Hydro Dynamics (MHD), and it deals with the conversion of electromagnetic energy into mechanical work in fluid media [1, 2]. To date, MHD has mostly been used to pump and control highly conducting fluids such as liquid metals and ionized gases, to study ionospheric/astrophysical plasmas, and to control magnetic fusion devices. The potential use of electromagnetic forces in microdevices has attracted much less attention. Recently, a number of researchers constructed MHD micro-pumps in silicon [3, 4] and ceramic substrates [5] and demonstrated that these pumps are able to move liquids around in micro conduits. MHD can be used not only for the purpose of pumping fluids but also to induce secondary complex flows, including chaotic advection that may be beneficial for stirring and mixing [6-9]. In this paper, we propose to go one step further. By equipping individual branches of a network with MHD drives, one can direct the fluid to follow any desired path without a need for mechanical valves and pumps. In other words, by controlling the voltages or electric currents applied to the various branches of the network, one can direct the fluid flow analogously to directing electric current flows in electrical circuits.

We start by briefly describing the building blocks of the MHD network. These include "pumping elements" that can double as stirrers. Second, we develop a linear graph-based theory for the analysis and control of MHD fluidic networks. The graph theory presented here is an extension of theories used in the analysis of pipe networks (without Lorentz forces) [10, 11]. Using the topological properties of the network, the graph theory allows us to assemble and analyze the equations that relate the flow rates to the pressures and Lorentz forces in a systematic and economic manner. The graph theory approach also allows us to formulate and solve an optimal control problem pertaining to the specification of the potentials or the currents needed to achieve desired flow conditions. Third, we

describe briefly the branches' operation as stirrers capable of inducing chaotic advection. This section is a summary of material that we published in detail elsewhere [7-9], and it is included here for completeness. Subsequently, to demonstrate that the ideas described here can, indeed, be put into practice, we describe the fabrication and operation of a simple MHD network. Although the MHD networks can be fabricated with various substrate materials ranging from silicon to polymers, we used low temperature, co-fired ceramic tapes because they are dielectric and amenable to layered manufacturing, which facilitates the integration of hydraulic conduits and metallic paths in a three-dimensional setting, and because they provide a means for inexpensive, rapid prototyping.

2. THE BASIC BUILDING BLOCK

The basic building block (or branch) of the fluidic network is a conduit equipped with two electrodes deposited along opposing walls. Fig. 1 depicts schematically (not drawn to scale) the top view (a) and the cross-section (b) of such a conduit. The conduit need not be straight; but we assume that the radius of curvature is large compared to the conduit's width. The conduit has a rectangular cross-section of height (h) and width (W) aligned in the x_2-x_3 plane, and its length is L (L>>W). The coordinate x_1 is directed along the conduit's axis. Perfectly conducting electrodes (denoted C_U and C_D) are deposited along the two opposite sides of the conduit. Various arrangements of the electrodes can be envisioned. See Fig. 2. In the main body of the paper, we assume that the electrodes cover the sidewalls' entire height at $x_2=\pm W/2$ (Fig. 2a). In the actual device that we describe later, the electrodes were deposited on the conduit's bottom along the sidewalls, and they did not cover the entire height of the walls (Fig. 1b). The theory can be readily modified to handle this case as well as any other positioning of the electrodes (i.e., Figs. 2b and 2c). In Appendix A, we briefly analyze the situation that prevailed in our experiments (Fig. 1).

In addition to the electrodes C_U and C_D, some of the branches may be equipped with disk-shaped electrodes deposited along the centerline of their floors. In Fig. 1, these "point" electrodes are denoted A_i, where $i=1, 2,\ldots$. The "point" electrodes are used for stirring, and their function is explained in section 5. Electrodes C_U and C_D occupy length $L_e<L$. $(L-L_e)$ is sufficiently large to prevent significant "cross talk" between adjacent network elements. The conduit is filled with a liquid of electrical conductivity σ and viscosity μ. The liquid needs to be only slightly conductive. Of course, higher conductivity liquids are desirable as they facilitate low voltage operation and low ohmic heating. The electrodes are subjected to either an externally controlled potential difference (V) or current (I). The conduit is sufficiently long so that fringe effects can be neglected, and the current flow is essentially one-

dimensional. The conduit is placed in a uniform magnetic field of flux density $\mathbf{B} = B\hat{e}_3$ directed in the x_3-direction. Alternatively, one can use synchronized, alternating electric and magnetic fields. Far from the conduit's ends, Ohm's law for a moving conductor of conductivity σ in a magnetic field is:

$$\mathbf{J} = \sigma\left(-\nabla V + \mathbf{v}\times\mathbf{B}\right), \tag{1}$$

where **v** is the velocity vector, $v(x_2,x_3)$ is the velocity component in the x_1-direction, and $\mathbf{J}=J\hat{e}_2$ is the current's density. Bold letters denote vectors. The interaction between the electric current and the magnetic field generates a Lorentz force of density $\mathbf{J}\times\mathbf{B}$ in the x_1-direction. To the first approximation, we assume that the electrodes are relatively long, L>>W, and the fluid flow is fully developed ($\frac{\partial}{\partial x_1} = 0$) along most of the conduit's length. Later, we will comment about possible modifications that can be made in the model to accommodate developing flows. Assuming uniform current density, the time-independent Navier-Stokes equation in the x_1 direction for an incompressible, fully developed flow in a straight conduit is:

$$-\frac{dp}{dx_1} + BJ + \mu\left(\frac{\partial^2}{\partial x_2^2} + \frac{\partial^2}{\partial x_3^2}\right)v = 0 \qquad (-W/2<x_2<W/2,\ -h/2<x_3<h/2). \tag{2}$$

The axial velocity $v(x_2,x_3)$ satisfies the no-slip conditions at all solid walls: $v(\pm W/2,x_3) = v(x_2, \pm h/2)=0$. When the liquid is a weak conductor of electricity (such as saline solution), the term $\sigma B^2 v$ is small in comparison with $\sigma BV/W$ and can be safely neglected [5]. With the above approximation, equation (2) is similar to the classical problem of a fully developed, Poiseuille flow in a conduit with a uniform cross-section. White [12, page 123] provides an expression for the flow rate (Q) in a conduit with a rectangular cross-section of width (W) and height (h):

$$Q = \frac{hW^3}{12\mu}\chi\left(-\frac{dp}{dx_1} + k_1\frac{\sigma VB}{W}\right) = \frac{hW^3}{12\mu}\chi\left(-\frac{dp}{dx_1} + k_1 JB\right). \tag{3}$$

In the above, the series $\chi = \left(1 - \frac{192W}{\pi^5 h}\sum_{n=0}^{\infty}\frac{1}{(1+2n)^5}\tanh\left(\frac{(1+2n)\pi\, h}{2W}\right)\right)$ converges rapidly, and we replaced $-\nabla V = \frac{V}{W}$. When h>>W, χ→1, and equation (3) corresponds to flow between parallel plates. When the

current's density is uniform (Fig. 2a), k_1=1. When the current's density is not uniform, k_1 is a numerical coefficient of order one whose magnitude depends on the electrodes' size and placement. See Appendix A.

For our purposes, it is convenient to integrate equation (3) along the conduit's length to obtain:

$$Q_i = C_i \Delta p_i + M_i^{\,V} V_i , \tag{4}$$

where Δp_i is the difference between the upstream and downstream pressures. Alternatively, we can write a similar relationship in terms of the current (I):

$$Q_i = C_i \Delta p_i + M_i^{\,I} I_i . \tag{5}$$

In the above, $C_i = \dfrac{h_i W_i^{\,3}}{12 \mu_i L_i} \chi_i$ is the hydraulic conductivity, and $M_i^{\,V} = \dfrac{\partial Q_i}{\partial V_i} = k_{1,i} \dfrac{\sigma_i Le_i B}{W_i} C_i$ and $M_i^{\,I} = \dfrac{\partial Q_i}{\partial I_i} = k_{1,i} \dfrac{B}{h_i} C_i$ are the magneto-hydraulic "conductivities." The subscript (*i*) has been added to emphasize the fact that different conduits in the network may have different geometric dimensions and contain liquids with different properties. Witness that equation (5) is independent of the solution's electric conductivity. In the network, the pressure drop may not always be adverse to the flow. In some branches, the pressure may assist the flow while in others it may resist it.

Equations (4) and (5) represent linear relationships among the flow rate in each of the network branches, the pressure drop across each branch's length, the potential drop, and the current across the opposing electrodes. A linear relationship between the potential and the flow rate may not always hold [5]. One may need to use piecewise, linear approximations restricted to different ranges. In contrast, a nearly linear relationship between the flow rate and the current (equation 5) holds over the entire range of interest. In this sense, equation (5) is preferable to equation (4). The model (equations 4 and 5) can also be expanded upon to accommodate developing flows. In the latter case, C and M may depend on the flow rates, and the model will no longer be linear. Although the non-linear case can be handled using similar techniques to the ones described below, we focus in this paper only on the linear case.

3. ANALYSIS OF THE MHD FLUIDIC NETWORK

Many conduits, some or all of which are the type discussed in the previous section, can be linked together to form a network. The conduits may be arranged in a single plane or distributed in a multi-layered fashion. The entire device is subjected to a uniform magnetic field. The magnetic field can be generated externally with a permanent magnet or an electromagnet. Alternatively, the entire device can be fabricated within a magnetic material. A computer controls either the potentials or the currents supplied to various electrodes. By judicious adjustment of the electrodes' potentials or currents, one can direct the flow to follow any desired path at any desired flow rate without the need for mechanical pumps and valves.

In order to make the ideas concrete, we introduce the various definitions in the context of the simple network depicted in Fig. 3. This particular network was constructed to have just a few branches (N=6) in order to enable us to provide explicit expressions for the various terms that we introduce in this section while still maintaining the essential features of more extensive networks. An actual MHD network may have a very large number of branches. Each branch is similar to the conduit depicted in Fig. 1. Although the branches appear as straight lines in the schematic depiction (Fig. 3), the actual branches need not be straight. See Fig. 7 for an example. We assume, however, that the radius of curvature is large compared to the channel's size. The electrode pair of each branch is individually controlled. To the first order approximation, we assume that the electrical current is confined within each branch and that there is negligible cross talk (current leakage) among branches.

The network's (N) branches are denoted by the numbers 1, 2,….,6 in Fig. 3. The (k) nodes (vertices) are denoted with the letters a, b, .., e. Some of the nodes (a, c, and e) communicate with the outside world or with reagent reservoirs and serve as "sinks" and "sources." Q_a, Q_b, and Q_c denote the flow rates that go into and out of the network. It is possible for a network to have no sinks and sources (i.e., Fig. 7). For each branch, we write a constitutive law of the form of equation (4) or (5). When a branch does not contain electrodes, the hydro-magnetic conductivity is set to zero. For the network depicted in Fig. 3, we write six equations each relating the flow rate in a branch to the pressure drop along that branch's length and the potential difference across or the current between the electrodes. Additionally, mass continuity requires that all the flow rates arriving at each node sum up to zero. When the electrodes' potentials or currents are given, one can readily solve these equations to obtain the flow rates in all the branches. Although these equations are quite simple, in large networks, the task of assembling and solving these equations is cumbersome. Therefore, in various branches of engineering, it is common to use graph theory to

analyze large networks. Graph theory allows us to systematically and economically assemble the various equations associated with the network. Moreover, this theory also allows us to formulate an optimal control problem for the MHD network (section 4).

Linear graph theory has been used to analyze, among other things, flow in pipelines [10, 11] and electrical networks. Here, we modify this theory to enable us to analyze MHD networks. We start by adding fictional branches to the graph. To this end, we select one of the sink/source nodes as the reference (ground) node (i.e., node (a) in Fig. 3). In the absence of sinks and sources, we may select any of the nodes as the reference node. Since the fluid is incompressible and one is concerned only with the pressure differences, one can assign a zero value to the reference node's pressure. We connect all the other nodes to the reference node by drawing (k-1) fictional branches (denoted with dashed lines in Fig. 4 and assigned the numbers 7, 8, 9, and 10). Some of these artificial branches are used to convert the external links (sinks/sources) into internal links of the network, i.e, $Q_c=Q_8$ and $Q_e=Q_9$. The flow in all the other fictional branches (that do not connect sinks/sources to the reference node) is zero. It is not necessary to endow the fictional branches with hydraulic and magneto-hydrodynamic conductivities.

Each branch is assigned (arbitrarily) a direction indicated by an arrow. The flow in a branch is considered to be positive (negative) when it is in (opposed to) the direction of the arrow. A route, traced along the edges, that passes through any particular node only once is called a *path*. If, in a given graph, there exists a path between every pair of nodes, the graph is said to be *connected*. Here, we focus only on connected graphs. Any constituent part of the graph is a *sub-graph*. A *circuit* is a sub-graph that is connected and has only two distinct paths between every pair of nodes. For example, (1-7), (1-2-8), and (1-2-6-4-5) are circuits. A *cutset* consists of branches having the following properties: (i) when all of the branches of the cutset are removed, the graph splits into two unconnected subgraphs; and (ii) no subset of the cutset has property (i). In Fig. 4, branches (9, 4, 1, 7, 8) and (6, 2, 8) are examples of cutsets.

We refer to the fictional branches as the tree and the actual branches of the network as the chords. When one chord is added to a tree, one *fundamental circuit* is formed. For example, if we add the chord (6) to our tree, the fundamental circuit (6-8-9) will form. A cutset containing exactly one tree branch is called a *fundamental cutset*. Branches (7, 2, 3, and 1) form a fundamental cutset. Below, we will denote, respectively, the variables associated with the tree and the chords with subscripts (t) and (c). We denote, respectively, the number of tree branches and chords as $T_b=(k-1)$ and N. Typically, $T_b<N$. In Fig. 4, $\mathbf{\Delta p}_t^T=\{\Delta p_7, \Delta p_8, \Delta p_9, \Delta p_{10}\}$ is (T_b*1) vector; $\mathbf{\Delta p}_c^T=\{\Delta p_1, \Delta p_2,$

Δp_3, Δp_4, Δp_5, $\Delta p_6\}$ is (N*1) vector; $\mathbf{Q}_t^T=\{Q_7, Q_8, Q_9, Q_{10}\}$ is (T_b*1) vector; and $\mathbf{Q}_c^T=\{Q_1, Q_2, Q_3, Q_4, Q_5, Q_6\}$, $\mathbf{V}_c^T=\{V_1, V_2, V_3, V_4, V_5, V_6\}$, and $\mathbf{I}_c^T=\{I_1, I_2, I_3, I_4, I_5, I_6\}$ are (N*1) vectors. We have no need for $\mathbf{V}_t$ and $\mathbf{I}_t$.

According to Kirchhoff's law, the sum of the pressure differences around each fundamental circuit is equal to zero. We write below the fundamental circuit equations in matrix form for the network depicted in Fig. 4. We follow the circuit in the direction dictated by the direction of the flow in the chord.

$$
\begin{array}{c}
\\
\textit{chords}
\end{array}
\begin{array}{c}
\begin{array}{cccccc|cccc} \multicolumn{6}{c|}{\textit{chords}} & \multicolumn{4}{c}{\textit{tree branches}} \\ 1 & 2 & 3 & 4 & 5 & 6 & 7 & 8 & 9 & 10 \end{array} \\
\begin{array}{c} 1 \\ 2 \\ 3 \\ 4 \\ 5 \\ 6 \end{array}
\left[\begin{array}{cccccc|cccc}
1 & 0 & 0 & 0 & 0 & 0 & 1 & 0 & 0 & 0 \\
0 & 1 & 0 & 0 & 0 & 0 & -1 & 1 & 0 & 0 \\
0 & 0 & 1 & 0 & 0 & 0 & -1 & 0 & 1 & 0 \\
0 & 0 & 0 & 1 & 0 & 0 & 0 & 0 & 1 & -1 \\
0 & 0 & 0 & 0 & 1 & 0 & 0 & 0 & 0 & 1 \\
0 & 0 & 0 & 0 & 0 & 1 & 0 & 1 & -1 & 0
\end{array}\right]
\end{array}
\left[\begin{array}{c}
\Delta p_1 \\ \Delta p_2 \\ \Delta p_3 \\ \Delta p_4 \\ \Delta p_5 \\ \Delta p_6 \\ \hline \Delta p_7 \\ \Delta p_8 \\ \Delta p_9 \\ \Delta p_{10}
\end{array}\right] = 0 \qquad (6)
$$

More generally,

$$
\begin{bmatrix} I & S \end{bmatrix} \begin{bmatrix} \Delta \mathbf{p}_c \\ \Delta \mathbf{p}_t \end{bmatrix} = 0 . \qquad (7)
$$

In the above, I is a N*N identity matrix and S is a N*T_b topology matrix that contains only +1, -1, and 0 as its entries. For example, the last row of equation (6) sums the pressure heads around the circuit (6, 8, 9). We follow the direction dictated by chord (6). As we move around the circuit, any tree branch that is aligned in chord 6's direction is assigned the entry (+1) in S (i.e., tree branch 8). Any tree branch that is aligned in the opposite direction is assigned the entry (–1) (i.e., tree branch 9). Any tree branch that is not included in this particular circuit is assigned the entry (0).

Upon rearranging equation (7), we express the chord variables in terms of the tree variables:

$$
\Delta \mathbf{p}_c = -S \Delta \mathbf{p}_t \qquad (8)
$$

Using the fact that the sum of all the flows going to any node is equal to zero, we write the cutset equations. Each cutset equation contains only one tree branch. The flow is taken to be positive with respect to the node when it is in the same direction assigned to the tree branch with respect to the node.

$$\begin{array}{c} \\ \textit{tree branches} \\ \end{array} \begin{array}{c} \begin{array}{cccc|cccccc} \textit{tree branches} & & & & \textit{chords} & & & & & \\ 7 & 8 & 9 & 10 & 1 & 2 & 3 & 4 & 5 & 6 \end{array} \\ \begin{array}{c} 7 \\ 8 \\ 9 \\ 10 \end{array} \left[\begin{array}{cccc|cccccc} 1 & 0 & 0 & 0 & -1 & 1 & 1 & 0 & 0 & 0 \\ 0 & 1 & 0 & 0 & 0 & -1 & 0 & 0 & 0 & -1 \\ 0 & 0 & 1 & 0 & 0 & 0 & -1 & -1 & 0 & 1 \\ 0 & 0 & 0 & 1 & 0 & 0 & 0 & 1 & -1 & 0 \end{array}\right] \end{array} \left[\begin{array}{c} Q_7 \\ Q_8 \\ Q_9 \\ Q_{10} \\ \hline Q_1 \\ Q_2 \\ Q_3 \\ Q_4 \\ Q_5 \\ Q_6 \end{array}\right] = 0 \quad , \tag{9}$$

or, more generally,

$$\begin{bmatrix} I & -S^T \end{bmatrix} \begin{bmatrix} \mathbf{Q_t} \\ \mathbf{Q_c} \end{bmatrix} = 0 . \tag{10}$$

For example, the last row of equation (9) corresponds to the cutset consisting of the tree branch (10) and the chords (4) and (5). The equation sums the flows that go into node (d) in Fig. 4. Flows that are directed the same way as the flow in the tree branch with respect to the node are considered to be positive.

Upon rearranging equation (10), we express the tree's flow rates in terms of the chord flow rates:

$$\mathbf{Q_t} = S^T \mathbf{Q_c} \tag{11}$$

Next, we can proceed with either equation (4) or (5). The use of equation (5) is preferable as the relationship between the flow rate and the current is nearly linear. We rewrite equation (5) in matrix form:

$$\mathbf{Q}_c = C\Delta\mathbf{p}_C + M^I \mathbf{I_c} , \tag{12}$$

where C and M^I are N*N diagonal matrices whose diagonal entries are, respectively, the hydraulic and magneto-hydraulic conductivities. Upon substituting (11) into the constitutive relationship (12), we have:

$$\mathbf{Q_t} = -K\Delta\mathbf{p_t} + S^T M^I \mathbf{I_c} , \tag{13}$$

where the "stiffness" matrix $K=S^TCS$ is symmetric and positive.

When the flow rates in all the tree branches are known and the currents supplied to the electrodes $\mathbf{I_c}$ are specified, equation (13) can be readily solved for the pressure differences across the tree branches,

$$\mathbf{\Delta p_t} = K^{-1}\left(-\mathbf{Q}_t + S^T M^I \mathbf{I_c}\right), \tag{14}$$

thereby providing information on the pressures at the various nodes. Subsequently, one can use equation (8) to obtain $\mathbf{\Delta p_c}$ and then equation (12) to compute the flow rates in the chords:

$$\mathbf{Q_c} = CSK^{-1}\mathbf{Q}_t + \left(I - CSK^{-1}S^T\right)M^I \mathbf{I_c}. \tag{15}$$

More often, we are likely to know the pressures at the sources and sinks and the (zero) flow rates at the tree branches that are connected to nodes that are neither sinks nor sources. In that case, we need to use a mixed formulation. Let's denote the number of sinks and sources as $(1+T_S)$ with $T_S \geq 1$. In Fig. 4, we assume that Δp_8 and Δp_9 are given ($T_S=2$) and $Q_{10}=Q_7=0$. We need to determine Δp_7, Δp_{10}, Q_8, and Q_9. More generally, we decompose the vector $\mathbf{\Delta p_t}$ into two parts: $\mathbf{\Delta p_t'} =[\mathbf{\Delta p_t}^S \ \mathbf{\Delta p_t}^U]^T$, where $\mathbf{\Delta p_t}^S$ denotes the T_S known pressure drops associated with the sinks and sources (other than the reference node) and $\mathbf{\Delta p_t}^U$ denotes the (T_b-T_S) unknown pressure heads. $\mathbf{\Delta p_t'}$ is obtained by reordering the vector $\mathbf{\Delta p_t}$. This can be conveniently accomplished with the aid of the permutation matrix G, i.e., $\mathbf{\Delta p_t'}=G\mathbf{\Delta p_t}$. Likewise, we decompose the vector $\mathbf{Q_t}$ into two parts: $\mathbf{Q}_t^{'}=[\mathbf{Q_t}^U \ \mathbf{0}]^T$, where $\mathbf{Q_t}^U$ denotes the (T_S) unknown flow rates associated with the sinks and sources and $\mathbf{0}$ denotes the (T_b-T_S) known (zero) flow rates. In Fig. 4, $\mathbf{\Delta p_t}^S=[\Delta p_8 \ \Delta p_9]^T$, $\mathbf{\Delta p_t}^U=[\Delta p_7 \ \Delta p_{10}]^T$, and $\mathbf{Q_t}^U=[Q_8 \ Q_9]^T$. Accordingly, we permute equation (12) by pre-multiplying it with the permutation matrix G to rearrange its rows in the form:

$$\mathbf{Q_t}^{'} = -R\mathbf{\Delta p_t}^{'} + GS^T M^I \mathbf{I_c}, \tag{16}$$

where $R=GKG^T$, $G^T=G^{-1}$, $\mathbf{Q}_t'=G\mathbf{Q}_t$, and $\mathbf{\Delta p_t'}=G\mathbf{\Delta p_t}$. G is a matrix consisting of zeros and ones as its entries. When we wish to make Q_i the j-th entry in the modified vector $\mathbf{Q_t}'$, we set $G_{j,i}=1$ and all the other entries in row (i) equal to zero. In our example,

$$G = \begin{pmatrix} 0 & 1 & 0 & 0 \\ 0 & 0 & 1 & 0 \\ 1 & 0 & 0 & 0 \\ 0 & 0 & 0 & 1 \end{pmatrix}.$$

The system (16) can now be partitioned in the form:

$$\begin{pmatrix} \mathbf{Q_t}^U \\ \mathbf{0} \end{pmatrix} = -\begin{pmatrix} R_{11} & R_{12} \\ R_{21} & R_{22} \end{pmatrix}\begin{pmatrix} \mathbf{\Delta p_t}^S \\ \mathbf{\Delta p_t}^U \end{pmatrix} + GS^T M^I \mathbf{I_c}, \tag{17}$$

where R_{11}, R_{12}, R_{21}, and R_{22} are, respectively, T_S*T_S, $T_S*(T_b-T_S)$, $(T_b-T_S)*T_S$, and $(T_b-T_S)*(T_b-T_S)$ matrices. Isolating the unknown quantities, we have:

$$\begin{pmatrix} \mathbf{Q_t}^U \\ \mathbf{\Delta p_t}^U \end{pmatrix} = \begin{pmatrix} I & -R_{12}R_{22}^{-1} \\ 0 & R_{22}^{-1} \end{pmatrix}\left(-\begin{pmatrix} R_{11} \\ R_{21} \end{pmatrix}\mathbf{\Delta p_t}^S + GS^T M^I \mathbf{I_c} \right). \tag{18}$$

Once the unknown components of $\mathbf{\Delta p_t}$ and $\mathbf{Q_t}$ are calculated, the chord variables can be readily obtained by solving the equations (8) and (5*)*.

4. OPTIMAL CONTROL PROBLEM

Another interesting problem is the determination of the potentials or currents that are needed to achieve the desired flow rates in the various chords. This is essentially a control problem. Generally, this problem does not have a unique solution. There may be many different ways to achieve the desired flow rates. We wish to select the set of currents that is "optimal" in some sense. For example, it may be desirable to minimize the energy dissipation of the system. Let Ω be a diagonal matrix whose entries are the electric conductivities of the various chords. Ω_{ii} depends on the conduit's geometry and the electrolyte's electric conductivity, i.e., $\Omega_{ii} = k_2 \dfrac{\sigma_i Le_i h_i}{W_i}$. When the electrodes occupy the entire height of the side walls, k_2=1. In other cases, k_2 is a numerical coefficient of order 1 (see Appendix A). The objective function,

$$F = \mathbf{I}_c^T \, \Omega^{-1} \, \mathbf{I}_c, \tag{19}$$

represents the network's power dissipation. We need to determine $\mathbf{I_c}$ and $\mathbf{\Delta p_t}^U$ so as to minimize (F). To this end, we substitute (8) in equation (5) and append the resulting equation to (19) with the aid of the (N*1) Lagrange multiplier vector ($\boldsymbol{\lambda}$):

$$J' = \mathbf{I}_c^T \Omega^{-1} \mathbf{I}_c + \boldsymbol{\lambda}^T \left(\mathbf{Q}_c + \begin{pmatrix} U_1 & U_2 \end{pmatrix}\begin{pmatrix} \mathbf{\Delta p_t^S} \\ \mathbf{\Delta p_t^U} \end{pmatrix} - M^I \mathbf{I_c} \right), \tag{20}$$

where $U=(U_1\ U_2)=CSG^T$. Subsequently, by taking the variations with respect to $\mathbf{I_c}$ and $\mathbf{\Delta p}^U_t$ and equating the appropriate coefficients to zero, we obtain the equations:

$$\begin{pmatrix} 2\Omega^{-1} & -M & 0 \\ 0 & U_2^T & 0 \\ M & 0 & -U_2 \end{pmatrix} \begin{pmatrix} \mathbf{I_c} \\ \boldsymbol{\lambda} \\ \Delta\mathbf{p_t^U} \end{pmatrix} = \begin{pmatrix} 0 \\ 0 \\ \mathbf{Q_c} + U_1 \Delta\mathbf{p_t^S} \end{pmatrix}. \tag{21}$$

Equations (21) can now be readily solved to obtain the optimal $\boldsymbol{I}_c$ and the unknown pressure heads $\Delta\mathbf{p}_t^U$. In our example (Fig. 4), the system (21) consists of 14 equations with 14 unknowns. The network can be programmed to direct the flow to follow any desired path. The optimization problem may also be augmented with various constraints such as the requirement that the potential differences or currents in various conduits do not exceed a prescribed value.

5. NETWORK BRANCHES OPERATING IN A STIRRING MODE

In addition to acting as a pump, the fluidic element depicted in Fig. 1 can serve yet another important function, that of a stirrer. Since flows in microdevices are highly regular and one is deprived of the benefits of turbulence, mixing is a challenge. The diffusion time of macromolecules may be prohibitively long even when the lengths are measured in hundreds of microns. In this section, we briefly describe how any of the network branches can double as an efficient stirrer. Our objective here is to demonstrate the basic concept. We refer the interested reader to references [8, 9] for further details.

In order to operate the basic MHD element as a stirrer, it is necessary to re-wire the various electrodes. This can be done with computer-controlled relay actuators. We connect both electrodes C_U and C_D (Fig. 1) together to form the single electrode C. When a potential difference is applied across the electrodes C-A_3, say, current flows between the point electrode A_3 and the combined wall electrodes C. The interaction between the magnetic field and this current induces circulatory motion of the liquid with the center of rotation being located at electrode A_3. Fig. 5 depicts a flow visualization experiment in which a drop of dye was introduced into the fluid. In accordance with theoretical predictions, the dye traces a closed orbit around the electrode A_3. The figure demonstrates that by appropriate patterning of the electrodes, one can induce a secondary flow that transports material transversely across the conduit's width. This motion is, however, quite regular and may not provide effective stirring. In order to obtain more complicated flow patterns, we activate the electrodes C-A_3 for the time (t) interval $0<t<T/2$, electrodes C-A_4 for the time interval $T/2<t<T$, and then electrodes C-A_3 again, and so on in a periodic fashion (with a period T). The resulting alternating circulatory patterns induce chaotic advection whose complexity increases as the period T

increases [8, 9]. This phenomenon is best observed in a movie[1]. Fig. 6 depicts the spread of a blob of dye when the potential difference is alternated across two pairs of electrodes after 2 (a), 3 (b), 4 (c), 6 (d), and 20 (e) periods following the introduction of the dye. By engaging larger numbers of electrode pairs C-A_i, one can further increase the complexity of the chaotic advection and extend the fraction of the conduit that participates in the mixing process. In short, Fig. 6 illustrates that the network branches can readily double as stirrers.

6. FABRICATION OF AND EXPERIMENTS WITH A MHD NETWORK PROTOTYPE

To illustrate that the ideas described in section 3 can be put into practice, we constructed and tested a very simple prototype of a MHD network with low temperature, co-fired ceramic tapes (LTCC). Although the device can be fabricated with various materials, we chose to use LTCC technology because it facilitates inexpensive rapid prototyping, and provides a platform for the integration of passive electronics and fluidics.

6.1 FABRICATION

In their pre-fired (green) state, the ceramic tapes consist of oxide particles (i.e., alumina), glass frit, and organic binder (that can be made from photo-resist). The tapes are commercially available at thicknesses starting at 100μm$\pm$7%. One can cast, however, even thinner tapes. The green tapes are soft and pliable, and they can be readily machined by laser, milling, and photolithography (when the binder is photo-resist). Metallic paths can be either printed or processed photolithographically to form electrodes, resistors, conductors, and thermistors. Conduit sizes may range from ~10μm to a few millimeters. Upon firing, the organic binder burns out, the oxide particles sinter, and the tapes solidify. Many tapes (>80) can be stacked together, aligned, laminated, and co-fired to form monolithic structures with complex, three-dimensional mazes of fluidic conduits, electronic circuits, and electrodes. Glass windows and other materials can be readily attached to the tapes to facilitate optical paths. Multiple layers of coils can be embedded in the tapes to generate magnetic fields [13, 14]. Alternatively, the tapes themselves can be made of a magnetic material.

A prototype of the MHD network was fabricated with DuPont LTCC 951AX tapes that have a nominal (pre-fired) thickness of ~250μm. A top view (with dimensions) and an exploded view are depicted, respectively, in Figs. 7 and 8. The fabrication process consisted of blanking rectangular segments of tapes to a desired size. A few layers

[1] A video clip is available at http://www.seas.upenn.edu:8080/~bau/ MHD Chaotic Stirrer.mov

of tapes were laminated to form a part. The various parts were machined individually using a numerically controlled milling machine. Subsequently, electrodes and conductor paths were printed on the various parts.

Part 1 includes 1.1mm wide × 1.7mm deep flow conduits and soldering pads (DuPont 6134 solderable conductor). The soldering pads are connected through vertical vias (filled with DuPont 6141 via fill paste) to the various electrodes. The various branches of the network are denoted with numbers from 1 to 7. Relatively large conduits were fabricated to facilitate easy flow visualization. Part 2 provides the bottom wall of the conduits. Electrodes (DuPont 5734, Au paste) approximately 20μm thick × 2mm wide electrodes were printed on the surface of part 2. The gold electrodes were aligned with the conduits' edges in such a way that when layers 1 and 2 were attached, about 100μm of the electrodes' widths (along each side of the conduits' vertical walls) were exposed to the conduit. Each branch contained its own pair of electrodes. A gap separated the electrodes in adjacent branches. Silver conductors (DuPont 6145) were printed on both parts 2 and 3 to facilitate the connection of each electrode to the soldering pads located on the surface of part 1. We used here planar architecture (all the conduits are in a single plane). There is no difficulty, however, in introducing conduits in different planes to form a three-dimensional multi-layered structure.

Subsequent to the machining and printing, the individual parts were stacked, aligned, laminated, and co-fired to form a monolithic block. Although the device shown in Fig. 7 can be easily capped with either a ceramic or glass plate, we left the device open to facilitate easy access to the channels and enable dye injection for flow visualization.

The electrodes were connected via computer-controlled relay actuators and a D/I card (PCL-725, Advantech Co., Ltd.) to the terminals of two DC-power supplies (Hewlett Packard, HP 6032A). The relays were programmed to switch "on" and "off" in such a way that any electrode pair could be active at any given time. Additionally, the relays allowed for the switching of the polarity of any given pair of electrodes. Power was supplied to the electrodes either in controlled voltage or controlled current mode.

The conduits were filled with 0.3M saline solution. The device was placed on top of a neodymium (NdFeB) permanent magnet of approximate intensity B=0.4T (Edmund Scientific). Dye (Cole Parmer Instrument Co.) was injected at various locations to achieve flow visualization. The flow progression was monitored with a video camera.

6.2 SAMPLE CALCULATION

In this section, we compute the control parameters that are needed to achieve two different flow paths. Fig. 9 provides a schematic replication of the network shown previously in Fig. 7. The chords (the actual network branches) are depicted with heavy solid lines and are labeled with numbers ranging from 1 through 6. For brevity's sake, we combined branches 1 and 7 into a single branch that is now labeled as branch 1. The fictitious tree branches are depicted with dashed lines and labeled 7, 8, and 9. The nodes are labeled with the letters a, b, c, and d. Node (a) is selected as the reference (ground) node. In contrast to the network analyzed in section 3, the network in Fig. 9 has no sinks or sources. This network is very simple, and we could have easily calculated the control variables directly without resorting to the method described in section 4. Nevertheless, we will use this opportunity to provide yet another illustration of the optimal-control algorithm's application.

The topology matrix S is:

$$S^T = \begin{pmatrix} 0 & 1 & 1 & -1 & 0 & 0 \\ 0 & 0 & 0 & 1 & -1 & -1 \\ -1 & 0 & 0 & 0 & 1 & 1 \end{pmatrix} \tag{22}$$

Since all the pressures are unknown, we do not need the permutation matrix G. Accordingly, $U=U_2=CS$. We carry out the calculations for the actual dimensions of the device shown in Fig. 7. The conduits are of uniform height (h=1.7mm) and width (W=1.1mm). χ=0.57. We assume 0.3M saline solution with electric conductivity $\sigma = 2.65\,\Omega^{-1}m^{-1}$, B=0.4T, $\mu=10^{-3}$kg/m-s, k_1=0.16 and k_2=0.26. Since the experiments were conducted with uncapped (open) conduits, we carried out the calculations for closed conduits with double the height. Subsequently, the results are adjusted to the appropriate conduits' sizes. The conduits' lengths are:

$$L = 10^{-3}(77.5,\quad 9.8,\quad 29.4,\quad 10,\quad 22.5,\quad 22.5)\,m,$$

where the i^{th} component corresponds to the length of the i^{th} conduit. The matrices C, M^I, and Ω are diagonal, and their diagonal terms are listed below.

$$diag(C) = 10^{-8}(0.4,\quad 3.1,\quad 1.0,\quad 3.0,\quad 1.33,\quad 1.33)\frac{m^3}{Pa\cdot s},$$

$$diag(M^I) = 10^{-7}(0.73,\quad 5.77,\quad 1.92,\quad 5.65,\quad 2.51,\quad 2.51)\frac{m^3}{A\cdot s},$$

and

$$diag(\Omega) = 10^{-1}(1.48,\quad 1.88,\quad 5.63,\quad 1.92,\quad 4.31,\quad 4.31)\Omega^{-1}.$$

In our first example, we wish to circulate the fluid around the torus (branches 2-3) with a flow rate of q_0=0.75μL/s. This corresponds to an average fluid velocity of 0.4mm/s. The flow rate vector is:

$Q_c = q_0(0,\quad 1,\quad -1,\quad 0,\quad 0,\quad 0)\frac{m^3}{s}$. Upon solving equations 21, we find that the currents that need to be applied to the various branches are: $I_c = (0\quad 1.3,\quad -3.9,\quad 0,\quad 0,\quad 0)m\text{A}$.

In the second example, we wish to direct the liquid along a path consisting of all the chords with the flow rates splitting between branches 2 and 3 and 5 and 6 in the proportions indicated below. The flow rate vector is: $Q_c = q_0(1,\quad 0.75,\quad 0.25,\quad 1,\quad 0.5,\quad 0.5)\frac{m^3}{s}$. The control currents are $I_c = (10.3,\quad 1.0,\quad 1.0,\quad 1.3,\quad 1.5,\quad 1.5)m\text{A}$. The total current needed to accomplish this task is 16.5mA. In both examples, there were no external pressure sources and all the conduits had the same magneto hydrodynamic conductivity. Moreover, in these example, all the nodes' pressures were the same. In general, however, the nodes' pressures will not be the same.

6.3 EXPERIMENTAL OBSERVATION

Our objective is to demonstrate that one can direct the fluid to follow any desired path by appropriate control of the currents supplied to the various electrodes. We monitored the fluid motion by injecting dye into the fluid and following the dye's progression. In one set of experiments, a trace of dye was inserted into the fluid at branch 1. The electrodes of all the branches were activated and the device was programmed to pump the fluid around the big loop (branches 1, 2/3, 4, and 5/ 6) with the flow splitting between branches 2 and 3 and 5 and 6. When the dye entered the torus (2-3), the electrodes of all the branches but 2 and 3 were switched off. The polarity of branch 3's electrodes was reversed, and the fluid was forced to circulate around the torus (2-3) a few times. One can imagine equipping the torus with different thermal zones such as may be needed for PCR. Subsequently, the polarity of electrodes in branch 2 was reset to its original setting, all the other electrodes were turned on, and the dye was pumped out of the torus into branch 4. The dye then split between branches 5 and 6 and recombined in branch 7. By appropriate choice of potential differences, the flow can be split between branches 5 and 6 in any desired

proportion or even made to circulate around the loop consisting of branches 5 and 6. This is just one example of a number of possibilities. An example of a flow visualization experiment was documented in a video clip[2].

In the experiments, we observed a nonlinear relationship between the current and the potential difference across the electrodes [5]. Likewise, the fluid velocity depended nonlinearly on the potential difference between the electrodes. When the applied potential was below a certain threshold value V_0~2.0V, very little current was transmitted in the solution. When the voltage was increased above V_0, both the current and the flow rate increased nearly linearly. The relationship between the flow rate and the current was, however, nearly linear over the entire domain of interest. Hence, the current is the preferred control variable.

Fairly large velocities on the order of cm/s can be attained. Since both the electromagnetic and the friction forces depend linearly on the length of the electrodes, the velocity is nearly independent of the length of the conduits. To the first order, the velocity-current relationship is also independent of the specific conductivity and molar concentration of the electrolyte solution.

When the current is maintained fixed, the velocity should remain fixed as well. This expectation is, indeed, supported by experiments. Fig. 10 depicts the fluid velocity as a function of time when the fluid circulated around the entire network, splitting between branches 2 and 3 and between branches 5 and 6. The total current supplied to the network was 15mA, and the approximate velocity was 0.4mm/s. The corresponding predicted value (see section 6.2) is 16.5mA. We speculate that this small discrepancy between the prediction and the experimental observation is attributable to the method that we used to measure the velocity. The fluctuations in the velocity as a function of time are well within our experimental error.

In our experiments, we encountered a number of potential problems such as bubble formation (at relatively high potentials) and electrode consumption. Another issue of concern is the possible migration of analytes in the electric fields induced by the electrodes. The severity of these undesired phenomena depends on the device's configuration and its intended duration of operation. Many of these problems can possibly be eliminated by appropriate design. For example, appropriate selection of electrolytes and electrode materials (redox species) and operation at sufficiently low potentials would prevent the hydrolysis of water and facilitate bubble-free operation. One can also operate with non-aqueous solutions. Electrode erosion is not likely to be a concern in disposable devices. Finally,

[2] A video clip of one such experiment is available at http://www.seas.upenn.edu:8080/~bau/. MHD network.mov

many of the adverse effects can be greatly reduced by operating with synchronized, alternating magnetic and electric fields (i.e., the various electrodes assume alternately the roles of cathodes and anodes) [4].

7. CONCLUSIONS

The paper demonstrated theoretically and experimentally that magneto-hydrodynamic forces can be conveniently utilized to propel and stir electrolyte solutions such as saline solutions in networks of conduits. MHD provides an attractive means for controlling liquid flow in a programmable way, without a need for mechanical valves and pumps, by prescribing either the potentials or the currents across electrode pairs. In other words, MHD allows one to control fluid flow in a fluidic network in very much the same way as potentials are used to control current flow in electrical networks.

We extended linear graph-based theory to enable us to compute systematically and economically the flow rates in various network branches when either the potentials or currents supplied to the electrodes are specified. The graph-based theory also facilitated the formulation of an optimal control algorithm that allows one to determine the electrodes' potentials or currents so as to achieve desired flow conditions (i.e., direct the fluid to follow any desired path). To demonstrate that the ideas articulated in this paper can be put into practice, we constructed and tested a simple prototype of a MHD network with low temperature, co-fired ceramic tapes (LTCC).

The tests results were in reasonable agreement with predictions and demonstrated that the theoretical ideas articulated in this paper are, indeed, practical. In the course of the experiments, we encountered, however, a number of problems (associated with the introduction of electric currents in electrolyte solutions) that require further research. These include electrode erosion, bubble generation (at relatively high electric potentials), and possible migration of analytes in the electric field. The severity of these problems depends on the intended use of the MHD networks. For example, electrode erosion and bubble generation may not be an issue with devices designed to operate for a limited amount of time. Bubble formation may not be a problem when one operates with open trenches. Furthermore, many of these problems may be either minimized or eliminated altogether through appropriate selection of electrolytes and electrode materials (i.e., the use of redox species) and/or through the use of synchronized, AC magnetic and electric fields [4]. Many other common means of propelling liquids in microdevices, such as electroosmosis, suffer from the very same drawbacks. MHD has, however, several

advantages such as ease of control, consistent and relatively high flow rates, insensitivity to surface properties, and low electrical potentials.

ACKNOWLEDGMENTS

The work described in this paper was supported, in part, by DARPA's SIMBIOSYS program (Dr. Anantha Krishnan, program director). DuPont has supplied us with free materials. A shorter version of this paper will be presented at the 2002 ASME International Mechanical Engineering Congress and Exhibition, November 2002.

APPENDIX A: The Flow Field in the Experimental Device

In the main body of the paper, we assumed that the electrodes occupy the entire surface area of the conduits' sidewalls (Fig. 2a). In contrast, in our experiments, the electrodes were about 50μm high, and they were printed along the conduits' sidewalls on the conduit's bottom (Fig. 1). As a result of this arrangement, the current flux and the Lorentz force were not uniform throughout the cross-section. In this appendix, we briefly investigate the effects of these non-uniformities on the flow field. The cross-section of the conduit is reproduced in Fig. A1. The conduit's aspect ratio is 1.55, b/W=0.55, and the relative height of the electrodes compared to the conduit's height is 0.03. The dark lines in Fig. A1 indicate the locations of the electrodes. We assume that the electrodes are equipotential surfaces. With the exception of the electrode surfaces, the conduit's walls are insulating. With the aid of a finite element package (FemLab), we solved the Laplace equation $\nabla^2 V = 0$ to calculate the potential V in this particular geometry. The current flux is proportional to the potential gradient, $-\nabla V$. Fig. A1 depicts the constant potential contours (solid lines) and the current flux (arrows). Not surprisingly, most of the current flows in the lower part of the conduit. The velocity profile of the flow induced by the Lorentz force was computed by solving the Poisson equation (2) with no pressure gradient. Figs. A2a and b depict, respectively, contours of constant axial velocity and the three-dimensional velocity profile. Recall that in our experiments, the top of the conduit was open. Thus, we used a free shear boundary condition at the conduit's upper surface. In contrast to the cases of uniform current and pressure-driven flows, the velocity profile attains its maximum value well below the conduit's center. By comparing the flow rates and the electrical resistance in the conduit depicted in Fig. A1 and in a conduit with a

uniform electric field (when the electrodes cover the entire area of the side walls), we find the coefficients k_1=0.16 (equation 3) and k_2=0.26.

REFERENCES

1. H. H. Woodson and J. R. Melcher, 1969, Electromechanical Dynamics, Vol. III, John Wiley.
2. P. A. Davidson, 2001, An Introduction to Magnetohydrodynamics, Cambridge.
3. J. Jang and S. S. Lee, 2000, Theoretical and Experimental Study of MHD (Magnetohydrodynamic) Micropump, Sensors and Actuators A, 80, 84-89.
4. A. V. Lemoff and A. P. Lee, 2000, An AC Magnetohydrodynamic Micropump, Sensors and Actuators B, 63, 178-185.
5. J. Zhong, M. Yi, and H. H. Bau, 2002, A Magneto Hydrodynamic Pump Fabricated with Low Temperature Co-fired Ceramic Tapes, Sensors and Actuators A Physical, 96, 1, 59-66.
6. H. H. Bau, J. Zhong and M. Yi, 2001, A Minute Magneto Hydro Dynamic (MHD) Mixer, Sensors and Actuators B, 79/2-3, 205-213.
7. H. H. Bau, 2001, A Case for Magnetohydrodynamics, Proceedings of the 2001 ASME International Mechanical Engineering Congress and Exhibition, New York, NY 2001.
8. M. Yi , S. Qian, and H. H. Bau, A Magneto-hydrodynamic (MHD) Chaotic Stirrer, to appear in the J. Fluid Mechanics.
9. Qian, Zhu, and Bau, A Stirrer for Magneto Hydro Dynamically Controlled Micro Fluidic Networks, to appear in Physics of Fluids.
10. Kesavan, H., K., and Chandrasekhar, M., 1972, Graph Theoretic Models for Pipe Network Analysis, J. of the Hydraulic Division, Proceedings of the American Society of Civil Engineers, 98, 345-364.
11. R. Gupta and T. D. Prasad, 2000, Extended Use of Linear Graph Theory for Analysis of Pipe Networks, Journal of Hydraulic Engineering, 126, 56-62.
12. F. M. White, 1974, Viscous Fluid Flow, McGraw Hill.
13. H. H. Bau, G. K. Ananthasuresh, J. J. Santiago-Aviles, J. Zhong, M. Kim, M. Yi, and P. Espinoza-Vallejos, 1998, Ceramic Tape-Based Systems Technology, Micro-Electro-Mechanical Systems (MEMS), DSC-Vol. 66, 491-498.

14. M. Kim, M. Yi, J. Zhong, H. H. Bau, H. Hu, and G. K. Ananthasuresh, 1998, The Fabrication of Flow Conduits in Ceramic Tapes and the Measurement of Fluid Flow Through These Conduits. Micro-Electro-Mechanical Systems (MEMS), DSC-Vol. 66, 171-177.

LIST OF CAPTIONS

1. The basic building block (branch) of the microfluidic network (top view, left, and cross-section, right). The figure is not drawn to scale. When the device is operating in a pumping mode, the potential differene is applied across electrodes C_U and C_D. When it is operating in a stirring mode, electrodes C_U and C_D are interconnected to form a single electrode (C), and the potential difference alternates among electrode pairs C-Ai.
2. Examples of various possible electrode arrangements. Embodiment (a) can be readily fabricated using magnetic tapes (in this case, the conduit will be rotated by 90 degrees). The theory developed in the main body of the paper is applicable to this geometry. Embodiment (b) can be machined in silicon and plastics using various vapor deposition techniques. Embodiment (c) can be fabricated using layered manufacturing and screen-printing (or photo-sensitive metallic inks). To enhance visibility, the sizes of the electrodes are exaggerated.
3. A schematic description of a fluidic network.
4. The modified network with branches added to connect all the nodes to a single (common) node (node **a** in our example).
5. Flow visualization of the circulatory motion induced when a potential difference is imposed across electrodes A_3 and C.
6. Dye traces formed when two electrode pairs i.e, A_3-C and A_4-C (in Fig. 1), are alternately engaged with a period T. In the first half of the period, A_3 and C were, respectively, connected to the positive and negative terminals of the power supply. In the second half of the period, electrodes A_4 and C were connected, respectively, to the negative and positive terminals of the power supply. (a) $t \approx 2T$ (b) $t \approx 3T$ (c) $t \approx 4T$ (d) $t \approx 6T$ (e) $t \approx 20T$
7. A photograph of the MHD fluidic network. The dimensions of the various features are given in the photograph.
8. Exploded view of the fluidic device depicting the various parts that were used in its construction. Part 1 was made of 8 ceramic layers, and it contains the flow conduits. Part 2 provides the bottom for the conduits and houses the electrodes needed to control the fluid flow. Part 3 contains the conductors that were used to connect the individual electrodes to the soldering pads located on the device's surface.
9. Schematic depiction of the network shown previously in Fig. 6. The chord and tree (fictitious) branches are depicted, respectively, with solid and dashed lines.
10. The fluid velocity as a function of time when the device is operating in a "controlled current mode." The total current supplied to the network is 15mA.

A1: The contours of constant potential (solid lines) and current flux (arrows) in the conduit's cross-section. The heavy lines indicate the locations of the electrodes.

A2: Contours of constant axial velocity (a) and the axial velocity profile as functions of x_1 and x_2.

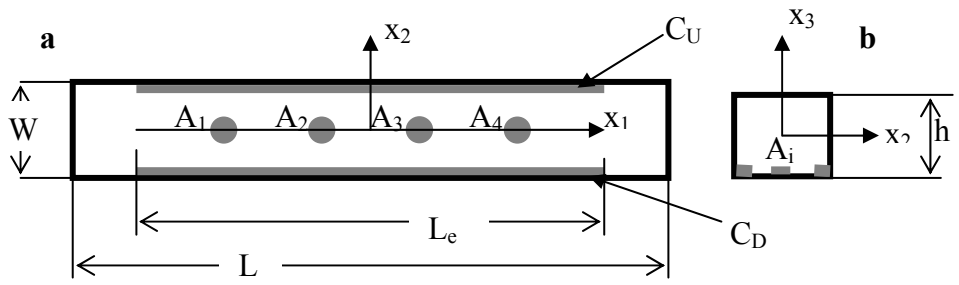

Fig. 1: The basic building block (branch) of the microfluidic network (top view, left, and cross-section, right). The figure is not drawn to scale. When the device is operating in a pumping mode, the potential differene is applied across electrodes C_U and C_D. When it is operating in a stirring mode, electrodes C_U and C_D are interconnected to form a single electrode (C), and the potential difference alternates among electrode pairs C-Ai.

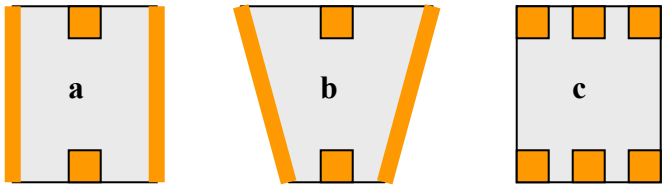

Fig. 2: Examples of various possible electrode arrangements. Embodiment (a) can be readily fabricated using magnetic tapes (in this case the conduit will be rotated by 90 degrees). The theory developed in the main body of the paper is applicable to this geometry. Embodiment (b) can be machined in silicon and plastics using various vapor deposition techniques. Embodiment (c) can be fabricated using layered manufacturing and screen-printing (or photo-sensitive metallic inks). To enhance visibility, the sizes of the electrodes are exaggerated.

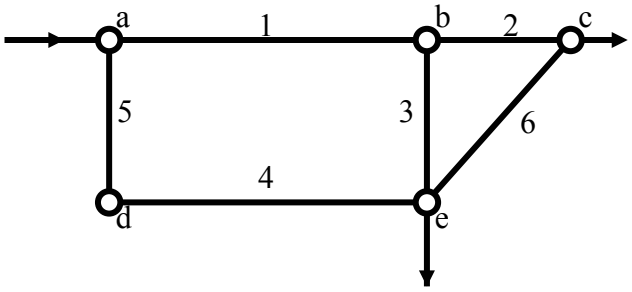

Fig. 3: A schematic description of a fluidic network

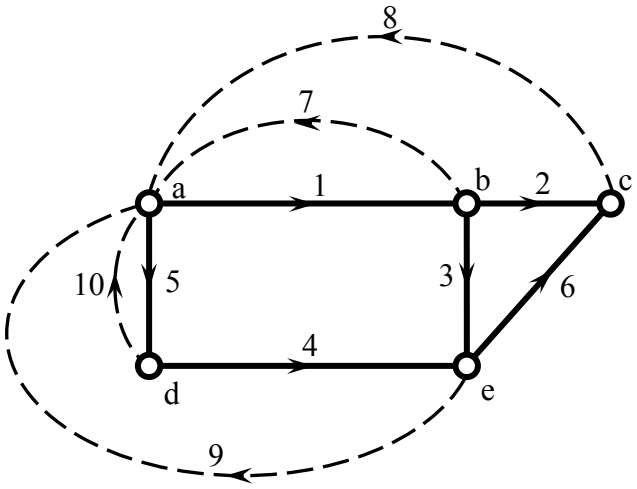

Fig. 4: The modified network with branches added to connect all the nodes to a single (common) node (node **a** in our example).

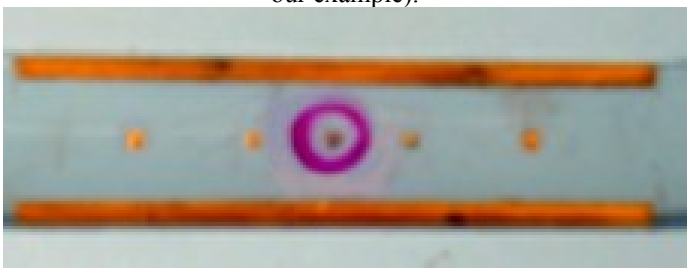

Fig. 5: Flow visualization of the circulatory motion induced when a potential difference is imposed across electrodes A_3 and C.

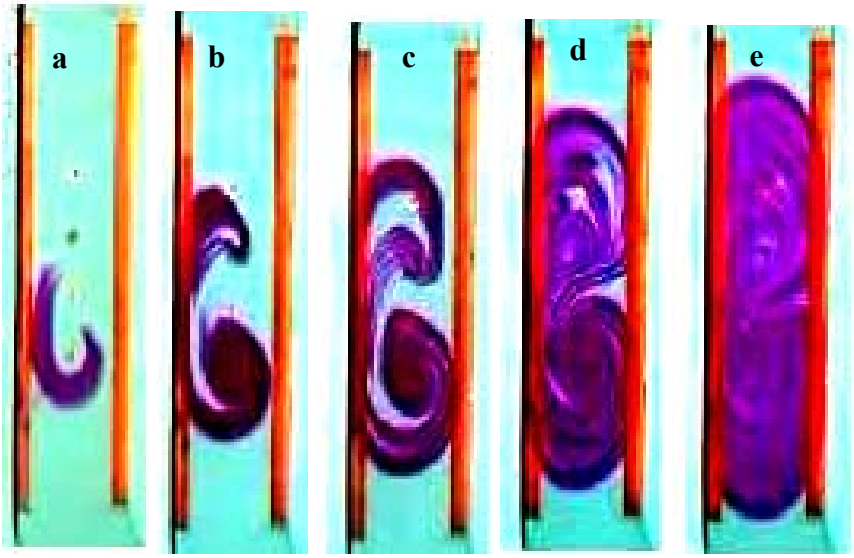

Fig. 6: Dye traces formed when two electrode pairs, i.e, A_3-C and A_4-C (in Fig. 1), are alternately engaged with a period T. In the first half of the period, A_3 and C were, respectively, connected to the positive and negative terminals of the power supply. In the second half of the period, electrodes A_4 and C were connected, respectively, to the negative and positive terminals of the power supply. (a) $t \approx 2T$ (b) $t \approx 3T$ (c) $t \approx 4T$ (d) $t \approx 6T$ (e) $t \approx 20T$

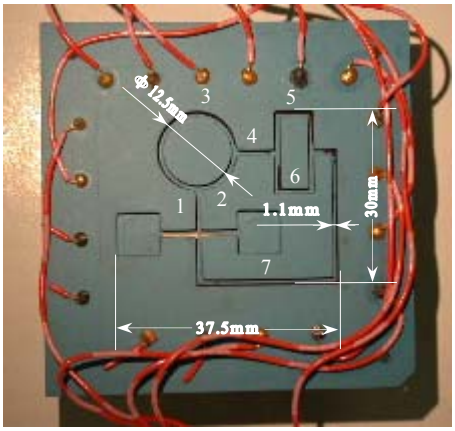

Fig. 7: A photograph of the MHD fluidic network. The dimensions of the various features are given in the photograph.

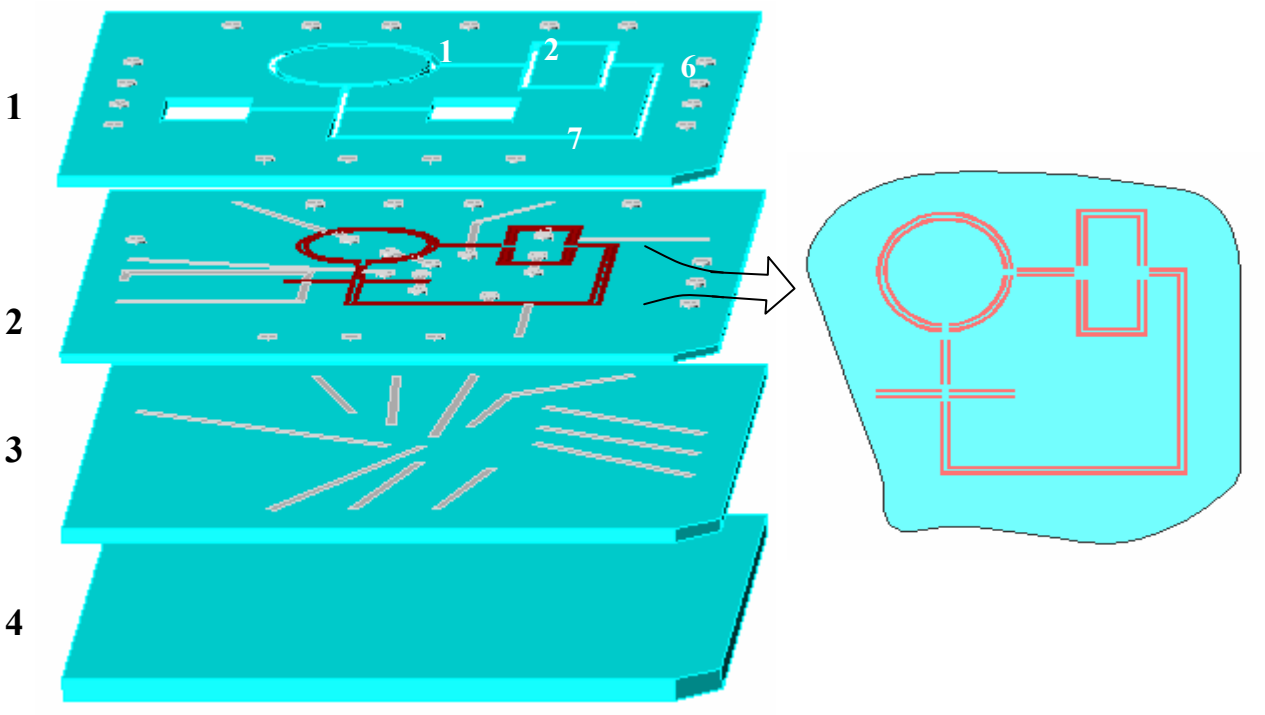

Fig. 8: Exploded view of the fluidic device depicting the various parts that were used in its construction. Part 1 was made of 8 ceramic layers, and it contains the flow conduits. Part 2 provides the bottom for the conduits and houses the electrodes needed to control the fluid flow. Part 3 contains the conductors that were used to connect the individual electrodes to the soldering pads located on the device's surface.

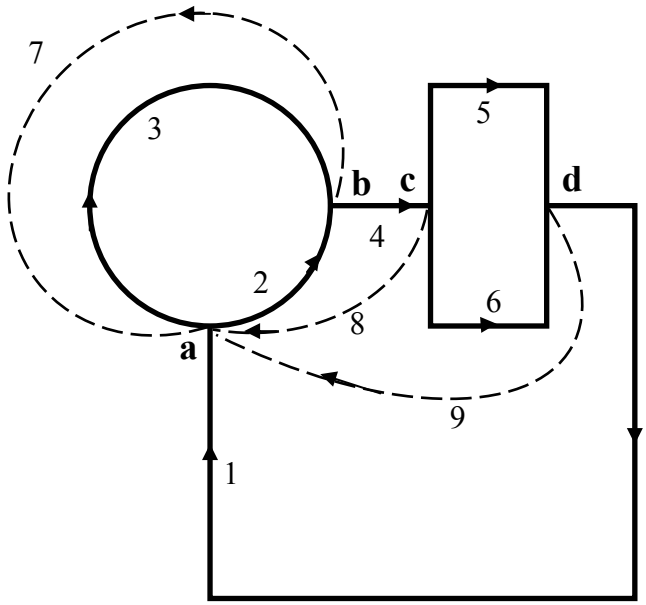

Fig. 9: Schematic depiction of the network shown previously in Fig. 6. The chord and tree (fictitious) branches are depicted, respectively, with solid and dashed lines.

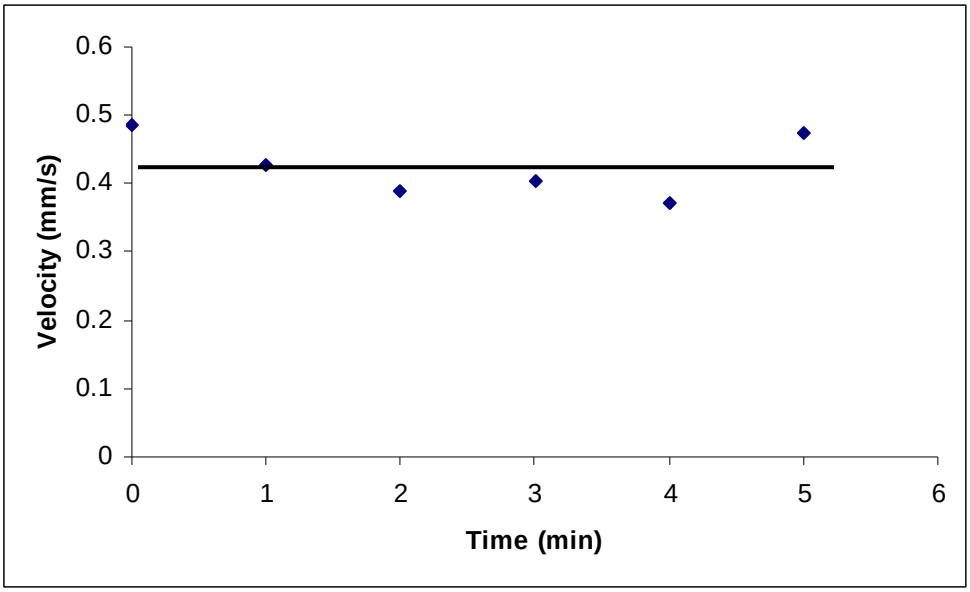

Fig. 10: The fluid velocity as a function of time when the device is operating in a "controlled current mode." The total current is 15mA.

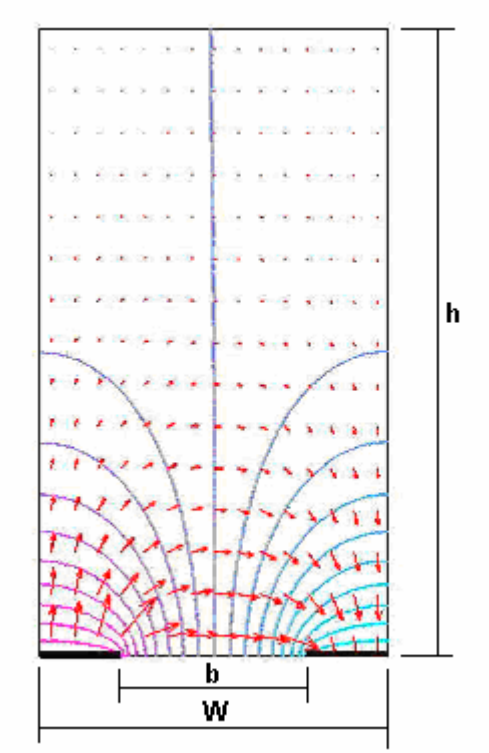

Fig. A1: Contours of constant potential (solid lines) and current flux (arrows) in the conduit's cross-section. The heavy lines indicate the location of the electrodes.

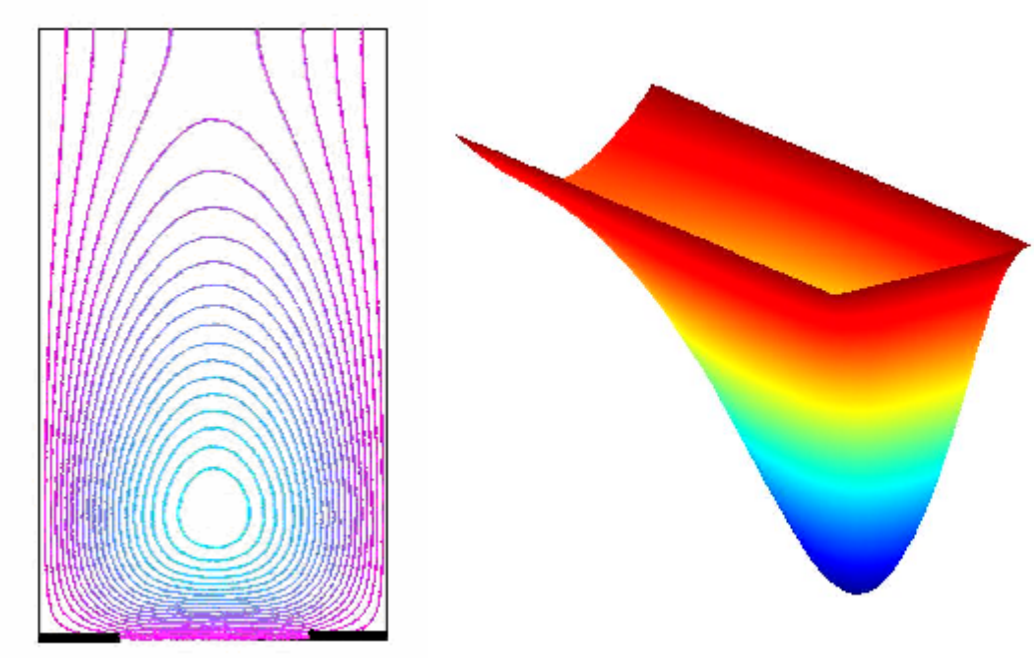

Fig. A2: Contours of constant axial velocity (a) and the axial velocity profile as a function of x_1 and x_2.